MDPI

Sensitivity Analysis of Bogie Wheelbase and Axle Load for Low-Floor Freight Wagons, Based on Wheel Wear

David S. Pellicer and Emilio Larrodé *

Department of Mechanical Engineering, University of Zaragoza, 50018 Zaragoza, Spain; dasapezu@unizar.es
* Correspondence: elarrode@unizar.es

Abstract: This paper shows the usage of a numerical analysis model that enables the calculation of the life of railway wheels used for low-floor freight wagons as a function of its primary operating factors, which allows for carrying out sensitivity analyses. Low-floor wagons are being increasingly used for combined transport applications, and many types of bogies have been proposed to constitute the wagons. Due to the uniqueness of this type of wagon, the bogie configurations in terms of wheelbase and axle load have hardly been analyzed so far. The numerical analysis model used addresses the primary challenges that arise in the vehicle–track interaction and establishes the relations among them. The main aspects of this model have been described in this paper, which has been later used to calculate the life of an ordinary-diameter wheel for several wheelbase and axle load values. This study has been replicated with reduced-diameter wheels, which are commonly used for low-floor wagons. In this way, it is possible to know the evolution of the life depending on the wheelbase and the axle load. The observed behaviors are not so dissimilar for the different types of wheels, and they point out huge increases in wear as the axle load and the wheelbase rise, especially with axle load. The root causes can be explained by the entire understanding of the rolling phenomenon provided by the full analytical work.

Keywords: sensitivity analysis; vehicle–track interaction; freight transport; sustainable transport; rail motorway

1. Introduction

The objective of this work is to determine the sensitivity of the wheelbase and axle load in wheel wear, which allows for establishing convenient configurations for the bogies with which low-floor wagons are equipped. For that, a theoretical calculation model able to determine the life of a wheel as a function of its primary operating factors is used. The model also allows for the variation in wheel diameter, which makes it possible to compare different types of wheels commonly found on these wagons. The work fully relies on the rail–wheel contact theory instead of on experimental data, but the theory has been validated by many scientists throughout decades of research.

Nowadays, the needs in the field of logistics are changing, and new transportation models are emerging. One of the models that has become more popular in the last years is the rail motorway model, which consists of transporting whole freight articulated vehicles on railway wagons. This model cuts down CO_2 emissions, saves fuel, reduces road congestion and may be more profitable than road transportation for some routes. It can also be used to skip certain obstacles, harsh routes or remote-access zones [1]. The concept of loading the whole heavy-duty vehicle avoids breakbulk shipping, whereas it brings the loading and unloading time down to 1 min since the vehicles can run on/off-board the wagons quickly, and then their wheels are also secured quickly [2]. Figure 1 shows a schematic diagram of this concept:
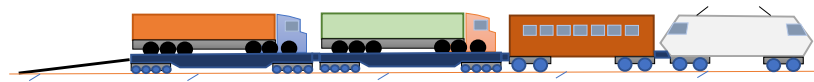
Figure 1. Concept described above. Source: own elaboration.

Notwithstanding, the adoption of this model often encounters the problem of loading gauge. Due to the height of the articulated vehicles used for road transportation, around 4 m [3], placing them on wagons leads to a further height increase over the rails that may conflict with the height limitations found in some tunnels or under some overpasses. Figure 2 illustrates the conflict: the European and Spanish loading gauges and their possible interferences with a rail motorway:
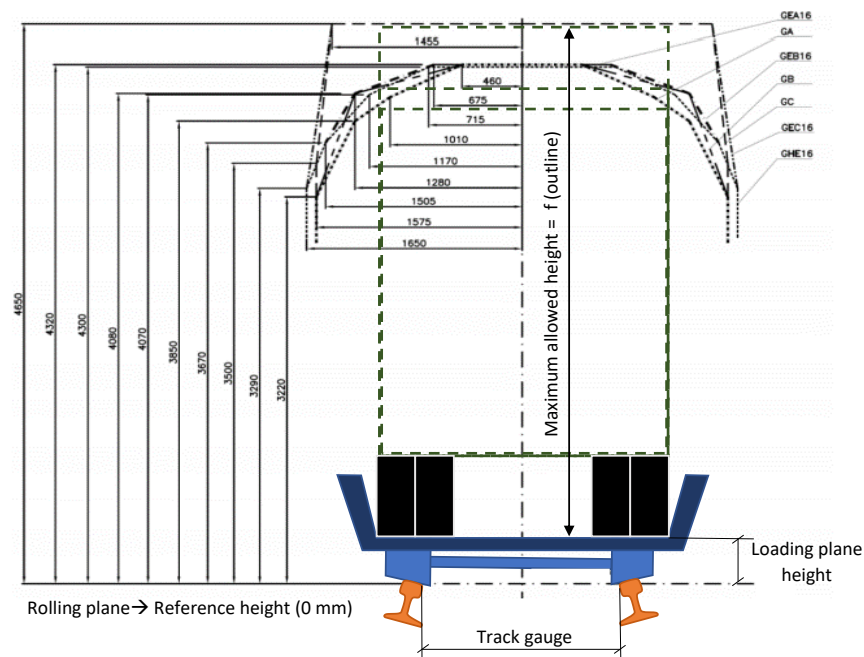

Figure 2. Illustration of the described conflict. Source: modification of a diagram from [4].

In order to avoid interferences between the load (the heavy-duty vehicles) and the civil structures (tunnels and overpasses found in the railway route) and keep transporting those road vehicles, there is one economically feasible alternative, as it does not require any civil works on the route: lowering the loading plane height. As can be seen in Figure 2, this height depends on the wheel diameter, among other factors, so it can be lowered by using reduced-diameter wheels [2].

An ordinary wheel has about 920 mm diameter, while a reduced-diameter wheel has a diameter value between half and a third of the ordinary one. From this variety of wheels, another variety of bogie originates. The wheels can be arranged on the bogies with different wheelbases, and they can be loaded more or less intensely, which, along with the number of axles, determines the axle load. This axle load is considered to be centered with respect to the wheelset center (Ref. [1] provides a ±10 value of load centering tolerance) and uniform across the wheelsets

For that, the calculation model sought must take into account many railway factors involved in vehicle–track interaction. These parameters can be grouped by wheel, wagon, railway superstructure, and external factors. The process consists of defining a mathematical model under the behavioral equations extracted from the models explaining wheel degradation, each of which includes a set of hypotheses. Additional hypotheses are formulated so as to take out the least influential factors on degradation. These hypotheses regard significant degradation phenomena as rolling contact fatigue (RCF).

Regarding the vehicle, the infrastructure and their interaction, the work aims to focus on the Spanish conventional railway network. This is because rail motorways are currently being fostered in Spain, and this country presents some obstacles to their implementation: the conventional railway network presents an unfavorable loading gauge [1], which prompts the adoption of low-floor wagons, and, additionally, the tight curves and the steep gradients inflict severe damage to wheels, being possible to mitigate it with smoother operating factors. These wheels are arranged in wheelsets, with a wheelset being the rigid union of an axle with a pair of wheels. Wheelsets are usually arranged in two-axle (two-wheelset) bogies and, according to the same reference, two bogies are enough for a flat-bed (and low-floor) wagon used on a rail motorway, so this is the type of railway vehicle that is to be considered for wheel degradation.

With that being said, the analysis is limited to freight transport and the Spanish national railway network, where the track gauge is specific: 1668 mm. The analysis excludes external factors such as the weather or the presence of pollutants, as these are fairly volatile and difficult to forecast.

This research paper can be compared to other cutting-edge work on wheel wear calculation but differs in some significant respects. These differences are commented upon next: To start with, Ref. [5] performs a sensitivity analysis with the key bogie parameters (suspension stiffness and wheel rolling radii difference, mainly) and uses the wear as an indicator, with the goal of reducing wheel flange wear and rail gauge corner wear and, thus, addressing the importance of wheel wear, although the rail vehicle modeled is an electric multiple unit (EMU) and axle load and wheelbase are not tackled. Ref. [6] carries out a sensitivity analysis of the primary suspension longitudinal clearance and stiffness and shows how significantly they can affect wear and increase maintenance costs, yet it does not deal with axle load and wheelbase. Ref. [7] shows the importance of addressing uneven wear and its impact on the railway system and the fact that reducing wheel diameter can impact wear patterns and dynamics, which is part of the theoretical foundation of the work hereby presented and has also performed the variation in axle load and wheelbase, differently to the former work. Ref. [8] emphasizes the relevance of considering the interaction between wheel and rail materials and their hardness in understanding wear behavior, which has been regarded in the current work, besides performing a sensitivity analysis. Ref. [9] found that the wear rate of materials with large total hardness used for the rail and wheel decreased, indicating a potential correlation between wheel diameter and wear rate, which has also been tackled in the current article, besides undertaking a sensitivity analysis. Refs. [10,11] stated that controlling and reducing friction and wear rate can be achieved through methods such as lubrication and load regulation, highlighting the effects of acceleration because of the impact of traction torque and creepages (load transfer phenomenon in suspension can make the wheel–rail interaction more intense than at a constant speed), albeit the current work focuses on sensitivity analysis with real axle load and also wheelbase values. Lastly, Ref. [12] simulates wear performance analysis using multibody simulation software and MATLAB, and the results indicate that the wheel wear rate increases proportionally with load; however, the work focuses on ordinary-diameter wheels and does not vary the wheelbase values.

The main contribution of this work consists in finding the evolution of wheel wear as a function of its operating factors for low-floor wagons, which have been hardly treated due to their uniqueness. The work is insightful, given that wheel, wheelset and bogie kinematics and dynamics are analyzed, so it provides comprehension as to why wheel life is not the same regardless of the parameters of interest and why dependencies exist.

Differently from the previous research, several realistic scenarios based on rail motorways are proposed, and only those parameters of interest were varied in the procedure of analysis developed, keeping the rest of the procedure the same or with equivalent parameters, which makes comparisons at the same level possible.

Once the procedure of analysis has been validated, the methodology is open to changes so that more factors can be added or some of the behavioral laws can be altered or swapped

in future research works in order to improve the accuracy and computational effort of the sensitivity analyses.

To conclude with the introduction, it is worth remarking that in order to carry out this research work, it has been necessary to review many analytical models that enable the calculation of wheel wear. Some of these models are based on rolling kinematics, while others are on dynamics. The most recurring Refs. are [13–21]. It is worth mentioning that [16] serves as a guide as it reviews the models and bridges the gaps between them by creating mutual interconnections and doing numerical checks when necessary. Additionally, those standards expedited by the Spanish Normalization Agency (AENOR) [22] and the Spanish Railway Infrastructure Manager (ADIF) [23], which are applied to rail–wheel interaction, have also been regarded to collect real data and know the actual restrictions.

2. Materials and Methods

This work follows a deductive method, as explained next:

First, the rail–wheel contact problem was studied based on the contact friction mechanics theory and the works and studies conducted since the second half of the 18th century. Thanks to this study, it was possible to choose the contact models with a higher accuracy and a lower computational cost: Hertz's solution, Polach's method, the center of friction, energy transfer and fatigue index, which were applied to tackle the main problems arising in the vehicle–track interaction.

These models include their own application hypothesis, but additional hypotheses are required in order to delimit the problem, so a series of hypotheses have been proposed. These hypotheses are fundamental in including important aspects or discarding aspects that will not have a significant impact on the problem solution.

Each of these models consists of a set of equations, which can be used to interrelate the models, so it is possible to construct a numerical analysis model in the form of an algorithm and program it on mathematical equation-solving software, which allows solving all of the equations after inputting the data required.

Then, the calculation scenarios are defined, and the data required by the algorithm are inputted. Running the algorithm with different input data is the base of the sensitivity analyses, conducted by varying the wheelbase and the axle load for wheels of different diameters.

Afterward, the results are plotted for all of the scenarios: the wheel life is obtained for different wheelbase and axle load values.

Finally, the results are compared and discussed, which allows for not only establishing convenient bogie configurations but also drawing conclusions about the influence of wheelbase and axle load on wheel wear.

2.1. List of Abbreviations

The abbreviations used in the article can be consulted in Table A1 for those with Latin symbols (Appendix A) and Table A2 for those with Greek symbols (Appendix A).

2.2. Hypthoteses

The following hypotheses were regarded besides the application hypotheses of Hertz's solution, Polach's method and wear calculation:

(a) The procedure is based on global calculations for the contact patch without discretizing it into finite elements.

(b) It is stationary; that is, it does not consider the variation in variables over time. At transition curves, where these variations are greater, mean values are computed.

(c) It disregards any rail wear and does not consider the previous wheel wear (it does not update the contact parameters as the profile wears out, but this profile is assiduously renovated).

(d) It is applied on all of the bogie wheels. For each wheel, the parameters and wear calculations are separately saved. This is because the wear is not the same for all of the wheels mounted on the same bogie [20].

(e)   It is applied on one bogie belonging to a wagon. A wagon normally consists of two bogies, but they can mostly rotate independently with respect to the other.

(f)   It disregards the tractive and compressive forces that some wagons transmit to the next ones through couplings when curving, which is due to the existing coupling slacks [15].

(g)   Creepage is obtained from a kinematic analysis of the wheelsets rather than from the non-dimensional slips.

(h)   In this kinematic analysis, the displacements from bogie suspensions and anti-yaw dampers are not included.

(i)   Only abrasive and adhesive wear are considered, without considering defects such as cracks, spalling, squats, flats, etc. [18,19].

(j)   RCF is only predicted without computing the extent of the damage produced, often sub-surface cracks [18].

(k)   The bogie wheels are considered to be non-powered, so $F_t = 0$ at the wheel–rail interfaces.

(l)   The bogie wheels are considered to be equipped with disk brakes, which do not wear the wheels out [16].

(m)   The railway vehicle is presumed to negotiate curves (circular or transition ones) at a constant speed, so it brakes (if necessary) before negotiating them; thus, $F_f = 0$ at a curve. There is an exception when the vehicle is running downhill, as explained in the next hypothesis.

(n)   The railway vehicle is assumed to brake slightly when running downhill, and reducing or cutting off traction is not enough to keep a constant speed at curves.

(o)   The infrastructure parameters that modify the wear conditions, such as warp, rail deflection, joints, impacts against switch frogs and track devices, and track irregularities, are not considered [14].

(p)   The influence of manufacturing or assembly tolerances of any element is not considered.

(q)   Axle load is considered to be centered with respect to the wheelset center and applied at a point with variable height, the center of gravity height (H_{CdG}). In fact, Ref. [1] provides a ±10 value of load centering tolerance.

(r)   Axle load is regarded as uniform; that is, all of the wheelsets composing a bogie share the same axle load.

(s)   By not considering rail deflection or manufacturing and assembly tolerances, it is possible to assume that the longitudinal rail curve radius ($R_{y,1}$) tends to infinity so that the associated curvature ($1/R_{y,1}$) tends to zero and can be taken as such.

(t)   The bogie wheels are assumed not to derail or block (this was numerically verified in [16]). Also, they are assumed not to displace laterally under cant deficiency or excess and low static friction conditions [16].

(u)   There are no hunting oscillations at the speed ranges considered (this was numerically proven in [16]).

2.3. Calculation Process

An algorithm consisting of input data blocks, calculation blocks and two output blocks was constructed. In Figure 3, input data blocks are represented in green, intermediate equation blocks are shown in blue (light for kinematics and dark for dynamics), and the output blocks are in purple. Regarding the symbols, the orange one with a diagonal cross inside represents the addition of values, the orange one with a Greek cross inside indicates a disjunctive, the gray one indicates that only one flow is inputted, and, finally, the yellow one is a bifurcation.
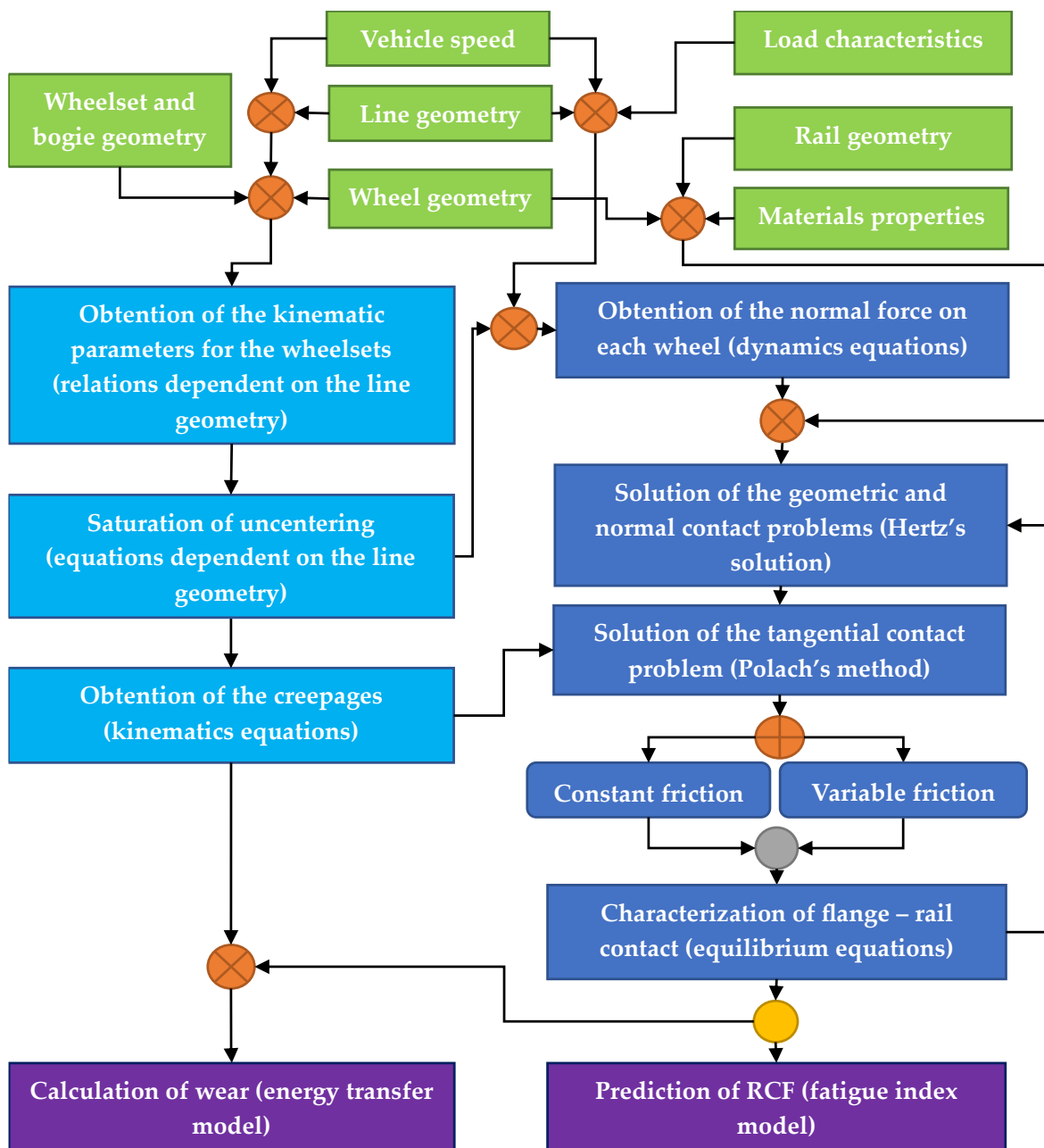
Figure 3. Flow diagram of the calculation process (algorithm). Source: own elaboration.

2.4. Calculation Model

The calculation model is defined in this subsection, starting with the definition of reference frames and following with the mathematical description of each of the equation blocks shown in Figure 3 (Section 2.3). The blocks belonging to the left main branch (those related to kinematics) are presented first, while the blocks of the right main branch (related to dynamics) are presented then.

2.4.1. Reference Frames Definition

Four reference frames were defined for the kinematics and dynamics analyses described in the next pages. These frames are described below and shown in Figure 4 for a wheelset (the whole bogie does not need a specific reference frame):

- Absolute reference frame *XYZ*, clockwise, fixed and whose origin is set on the rolling plane, anchored to the track beginning and centered between the rails.

- Track reference frame $\tilde{x}\tilde{y}\tilde{z}$, clockwise, mobile at the vehicle speed and whose origin is set on the rolling plane and along the track middle line, holding the $\tilde{x}$ axis always tangent to that line.
- Axle reference frame $\bar{\bar{x}}\,\bar{\bar{y}}\,\bar{\bar{z}}$, clockwise, mobile at the axle speed, and whose origin is set at the gravity center of the wheelset.
- Contact area reference frame $x_c y_c z_c$, clockwise, mobile at the contact area speed, and whose origin is set in the center of the area.
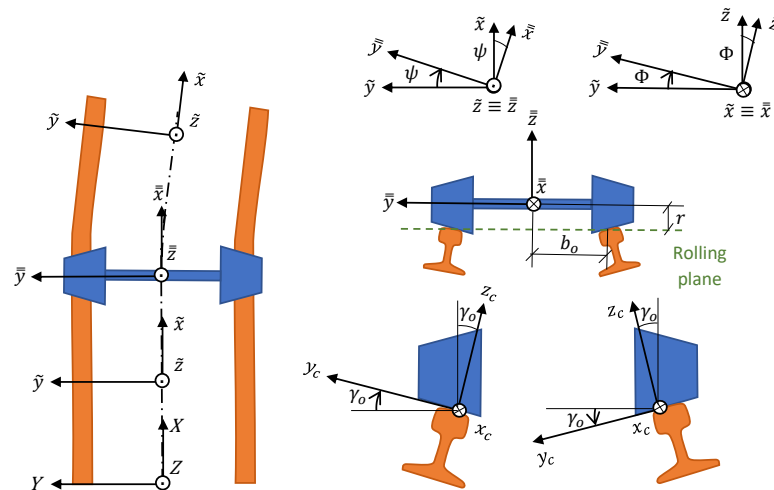

Figure 4. Reference frames definition. Source: own elaboration.

2.4.2. Kinematics Equations Blocks

Refs. [13,15,17,18,20,21] explain how to obtain the kinematic parameters for the wheelsets through relations dependent on the railway line geometry. Not only does Ref. [16] collect these relations, but it also extends them to all of the possible geometries that can be found in a railway line: straight section, circular curve and transition curve (clothoid, quadratic parabola or cubic parabola).

The parameters obtained at these geometries are described in Ref. [16]: uncentering and uncentering speed, average uncentering and uncentering speed, yaw angle and yaw angle variation speed/rate, average sinus of yaw angle and of yaw angle variation, average yaw angle, a combination of the uncentering and yaw angle effects, angle of longitudinal displacement of the contact area, and tilt and tilt speed/rate.

As explained in Refs. [17,18,20,21], the total uncentering of a wheelset (y^*) can be computed by adding the original uncentering and the uncentering coming from wheelset rotation (this rotation is, in reality, that of the bogie pivot with respect to the tangent line to the track centerline).

The reason why uncentering must be saturated is that there exists a geometrical constraint: total uncentering cannot be greater than the addition of half the track play/slack (the so-called "flangeway clearance") and the existing gauge widening (equal or different to 0). When total uncentering reaches that value, then the flange belonging to the outer wheel touches the outer rail.

Regarding the creepages, they are the rigid slip velocities divided by the vehicle speed in order to turn them into non-dimensional (although the spin creepage is dimensional as the resulting units are "rad/m"). Refs. [13,18,21] explain how to compute creepage from kinematics parameters, whereas Ref. [16] collects this information and proves the formulae. The creepages can be longitudinal, lateral and spin, as explained below:

1. Longitudinal creepage: Difference between the nominal wheel radius and the real rolling one (generating V_x^I), application of tractive or braking torques to the wheel (V_x^{II}) and variation in yaw angle (V_x^{III}).

2. Lateral creepage: Not null yaw angle (generating ΔV_y^I), adoption of a new equilibrium position by the wheelset (ΔV_y^{II}) and not null tilt angle (ΔV_y^{III}).

3. Spin creepage: Conicity (generating $\Delta \Phi^I$, alternatively known as the camber effect [18]) and variation in yaw angle (generating $\Delta \Phi^{II}$).

Finally, Figure 5 shows how a wheelset is positioned on a narrow curve where there is an uncentering limit imposed by geometrical constraints (for Iberian gauge, J = 1668 mm and *no.* = 20, so $\frac{J}{2}$ = 884 mm). Its main kinematics parameters are also shown. Below the figure, the main kinematics equations are presented: uncentering (1), its saturation (2)–(5), creepages definition (6)–(8), longitudinal creepage (9)–(11), transversal creepage (12)–(14) and spin (15)–(17):
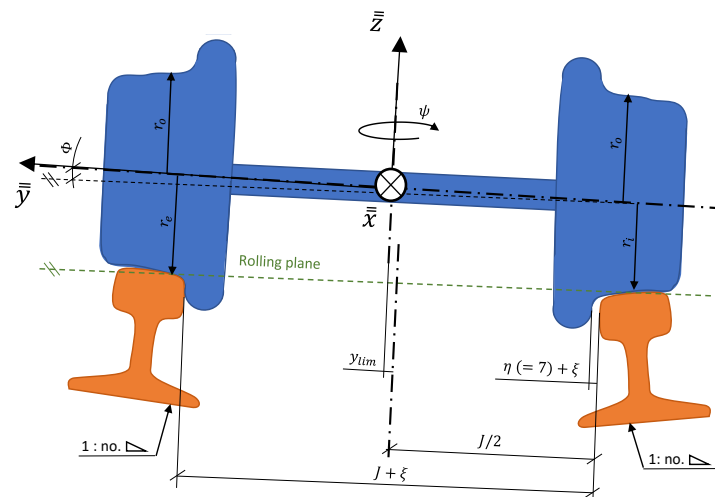
Figure 5. Wheelset positioning on a narrow curve. Source: own elaboration.

$$y = \frac{r_o b_o}{kR} \tag{1}$$

$$y^* \left(1^{st}\ wheelset\right) = y + e\frac{\pi\ |\psi|}{360} \tag{2}$$

$$y^* \left(2^{nd}\ wheelset\right) = y - e\frac{\pi\ |\psi|}{360} \tag{3}$$

$$y_{lim}^* = \frac{\eta}{2} + \xi \tag{4}$$

$$y^* = y_{lim}^*\ (\text{if the former was greater before}) \tag{5}$$

$$v_x = \Delta V_x / V \tag{6}$$

$$v_y = \Delta V_y / V \tag{7}$$

$$\varphi = \Phi / V \tag{8}$$

$$\Delta V_x = V_x^I + V_x^{III} + V_x^{III} \tag{9}$$

$$\Delta V_x = -\Delta r\ \omega - r_o \omega' \pm b_o \dot{\psi} \tag{10}$$

$$v_x = \frac{-\Delta r}{r_o} + \frac{-r_o \omega' \pm b_o \dot{\psi}}{V} \tag{11}$$

$$\Delta V_y = V_y^I + V_y^{III} + V_y^{III} \tag{12}$$

$$\Delta V_y = -V sen\psi\ cos\gamma_o + \dot{y}cos\ \gamma_o - r_i \dot{\Phi}cos\ \gamma_o \tag{13}$$

$$v_y = \left(-sen\psi + \frac{\dot{y} - r_i \dot{\Phi}}{V}\right)cos\gamma_o \tag{14}$$

$$\Delta\Phi = \Delta\Phi^I + \Delta\Phi^{II} \tag{15}$$

$$\Delta\Phi = \pm\omega\,sen\gamma_o + \dot{\psi}\cos\gamma_o \tag{16}$$

$$\varphi = \pm\frac{sen\,\gamma_o}{r_o} + \frac{\dot{\psi}\,cos\gamma_o}{V} \tag{17}$$

2.4.3. Dynamics Equation Blocks

The normal force is exerted by the rail on the wheel as a response to the opposite force (due to gravity or components of accelerations such as the centrifugal one) that the latter exerts on the former. Refs. [13,15,20,23–27] provide some information on how to compute the normal force on each wheel.

However, the most important Ref. is [16], as it is the one which fills the gaps and obtains the normal force on each wheel as a function of these factors: axle load (λ_{eje}), center of gravity of the axle load (H_{CdG}), gradient angle (β_{rp}) (directly inferred from the inclination (i)), cant angle (ϑ_r), lateral acceleration (a_{lat}), and wheel contact angle (γ_o) and longitudinal displacement angle of the contact patch (ς). This allows for obtaining the normal force on the outer and inner wheel in relation to a curve (N_e and N_i, respectively) and decomposing it into their perpendicular and parallel components ($N_\perp$ and $N_\parallel$). It should be noted that in a straight section, N_e and N_i would be identical (N).

On the other hand, an isolated wheel transmits its own weight and its load to the rail, which shares an interface: the contact area. The contact area must be greater than zero in order to avoid infinite normal stress. Both the contact area (geometry problem) and the normal stress must be determined so as to compute the wear and know where it acts (normal problem). As explained in Ref. [21], whenever two bodies make contact, that contact can be non-conformal or conformal. In the first type of contact, the contact area is relatively small in comparison with the characteristic size of the bodies, while in the second type of contact, the geometry of a body adapts to the geometry of the other body, resulting in a relatively big contact area (this could happen when the wheel and rail are so worn-out that their geometries coincide). Conformal contacts can be further simplified if the quasi-identity relation is fulfilled, which means that a relation between the shear modulus and the Poisson's ratio exists; this condition is fulfilled in this case, given that the materials in contact are the same (steel).

Both the geometric and the normal contact problems are solved together and in Refs. [18,20,21], these theories for solving them are commented upon. As stated in Ref. [16], which collects the theories, the Herztian contact theory is the most common due to its high accuracy and low computing effort and because the hypotheses it brings are fulfilled for most of the cases:

1. The bodies in contact are homogeneous, isotropic and linear elastic.
2. Displacements are supposed to be infinitesimal (much smaller than the bodies' characteristic dimensions).
3. The bodies are smooth at the contact zone, that is, without any roughness.
4. Each body can be modeled as an elastic half-space, which requires non-conformity.
5. The bodies' surfaces can be approximated by quadratic functions in the vicinity of the maximum interpenetration point. This implies that the curvatures (the second derivates of the functions) are constant.
6. The distance between the undeformed profiles of both bodies at the maximum interpenetration point can be approximated by a paraboloid.
7. The contact between the bodies is made without friction, so only normal pressure can be transmitted.

More details on Hertz's solution (theory, parameters, equations, etc.) are given in Refs. [28,29]. The equations of Hertz's model are appended at the end of the paper and range from A1 to A10 (Appendix B).

Nonetheless, the Hertzian model ignores the forces and torques due to friction; as a consequence of the relative motion between the wheel and the rail in the longitudinal and lateral directions and around the vertical axis (z_c), opposing forces and torques appear. These are associated with tangential stresses and deformations at the contact area, specifically at the slip region of the ellipse (split into one stick and one slip region). There are two ways to compute these variables:

- Analytical: The values are globally computed for the whole contact patch. A set of analytical equations are used, and the tangential problem can be decoupled from the geometric and normal ones because non-conformity and quasi-identity are satisfied.
- Finite-element: The values of the variables are locally computed and are added thereafter so as to obtain the global values. For that, the contact patch is meshed.

In the current work, the analytical method is chosen because it allows for tackling the problem with an algorithm that results in a good accuracy–computational effort ratio. For the computation of these tangential forces and the spin torque, in Refs. [18,20,21] some models are commented upon. Ref. [16] collects them, concluding that Polach's method is the most appropriate for considering the spin effect since it brings accurate results with a low effort.

Ref. [16] collects all of these theories and concludes that Polach's method is the most appropriate for considering the spin effect on the variables because it provides accurate results at a low computational effort. Refs. [30,31] provide more details on the method, which relies on Kalker's coefficients [32].

Another important part of dynamics is the flange–rail contact. This is an aggressive contact appearing at tight/narrow curves where gauge widening is not enough for a smooth curve negotiation, so the wheel flange presses laterally against the rail, and the rail exerts a reaction force on the flange. It is important to note that under the hypotheses considered, the tread–rail contact does not cease to exist.

To find the reaction that the rail exerts on the flange, Ref. [25] proposes the center of friction model. This model states that every bogie, when curving, has a point at which, if a wheel were mounted there, this wheel would spin ideally, that is, with no slip. This point is called the center of friction, and determining it allows computing the forces exerted by the rail on the flange–rail contact through force and torque balances. There can be one flange–rail contact (free motion) or two (restricted motion); the latter occurs at the tightest curves when the two wheels of a diagonal touch the rails.

Regarding the load distribution on the flange and the tread contact areas, Ref. [33] explains the Sauvage model, a heuristic method to obtain the total indentation (δ_o) as the sum of the indentation at the tread–rail contact (δ_{br}) and that at the flange–rail contact (δ_{pe}). Ref. [16] simplifies the Sauvage model by introducing the load distribution coefficient (α_{fn}), ranging from 0.5 (same normal load for both contacts) to 1 (the tread contact would become discharged). Its usual values are taken from the results of the Sauvage model: 0.7–0.8. Ultimately, this method is combined with the center of friction one.

Finally, Figure 6 shows the tangential forces and torques associated with the creepages at each wheel of a four-wheeled bogie. The main dynamics equations are introduced thereafter: those for normal force computation on each wheel (Equations (18)–(26)), those which allow applying Polach's method (Equations (27)–(35)) and, finally, those of the center of friction model (Equations (36)–(40)).

$$\lambda_{eje} = \frac{\lambda_u + \lambda_{tara}}{n_{ejes}} \tag{18}$$

$$H_{CdG} = \frac{\frac{1}{n_{ejes}}(\lambda_u H_u + \lambda_{tara} H_{tara})}{\frac{1}{n_{ejes}}(\lambda_u + \lambda_{tara})} \tag{19}$$

$$\beta_{rp} = arctan\left(\frac{i}{1000}\right) \tag{20}$$

$$\vartheta_r = arcsen\left(\frac{h_r}{2b_o}\right) \tag{21}$$

$$a_{lat} = \frac{V^2}{R+y} - \frac{h'_r}{2b_o} g\, cos\beta_r \tag{22}$$

$$N_e = \frac{\lambda_{eje}}{2}\left(1 + \frac{y}{b_o}\right) g\, cos\vartheta_r\, cos\beta_{rp} + \frac{\lambda_{eje}}{2b_o} a_{lat} H_{CdG} \tag{23}$$

$$N_i = \frac{\lambda_{eje}}{2}\left(1 - \frac{y}{b_o}\right) g\, cos\vartheta_r\, cos\beta_{rp} - \frac{\lambda_{eje}}{2b_o} a_{lat} H_{CdG} \tag{24}$$

$$N_\perp = N_{e|i} cos(\varsigma) cos(\gamma_o) \tag{25}$$

$$N_\parallel = N_{e|i} cos(\varsigma) sin(\gamma_o) \tag{26}$$

$$s_i = \frac{\mu N_\perp}{Gab\, C_{jj}} v_i, \quad i,j = x,1;\ i,j = y,2 \tag{27}$$

$$\begin{cases} s_{y,C} = s_y + (-\varphi)a, & |s_y + (-\varphi)a| > |s_y| \\ s_{y,C} = s_y, & |s_y + (-\varphi)a| \le |s_y| \end{cases} \tag{28}$$

$$F = -\frac{2\mu N_\perp}{\pi}\left(\frac{\varepsilon}{1+\varepsilon^2} + arctan\varepsilon\right) \tag{29}$$

$$F_i = F\frac{s_i}{s}, \qquad i = x,y \tag{30}$$

$$F_{y,S} = -\frac{9}{16}a\,\mu N_\perp\, K_M\left[1 + 6,3\left(1 - e^{-\frac{a}{b}}\right)\right]\frac{(-\varphi)}{s_C} \tag{31}$$

$$F_{y,C} = F_y + F_{y,S} \tag{32}$$

$$F = -\frac{2\mu N_\perp}{\pi}\left(\frac{k_A\varepsilon}{1+(k_A\varepsilon)^2} + arctan(k_S\varepsilon)\right) \tag{33}$$

$$\mu = \mu_o\left[\left(1 - A_f\right)e^{-wB_f} + A_f\right] \tag{34}$$

$$w_i = s_i V \qquad i = x,y \tag{35}$$

$$\zeta_v = \alpha_{fn} N_e \tag{36}$$

$$N_p = \zeta_v\, cos\gamma_o + \zeta_h\, sen\gamma_o \tag{37}$$

$$\left(-F_t\Big| + F_f\right) = -\sum_{i=1}^{i=Z_w+2} F'_{x,i} \tag{38}$$

$$\zeta_{h,1} - \zeta_{h,Z_w} = \sum_{i=1}^{i=Z_w+2} F'_{y,i} \tag{39}$$

$$\zeta_{h,1} u_{fl,1} - \zeta_{h,Z_w} u_{fl,4} = \sum_{i=1}^{i=Z_w+2}\left(F'_{y,i}\, u_{f,i}\right) + \sum_{i=1}^{i=Z_w+2}\left(F'_{x,i}\, v_{f,i}\right) \tag{40}$$
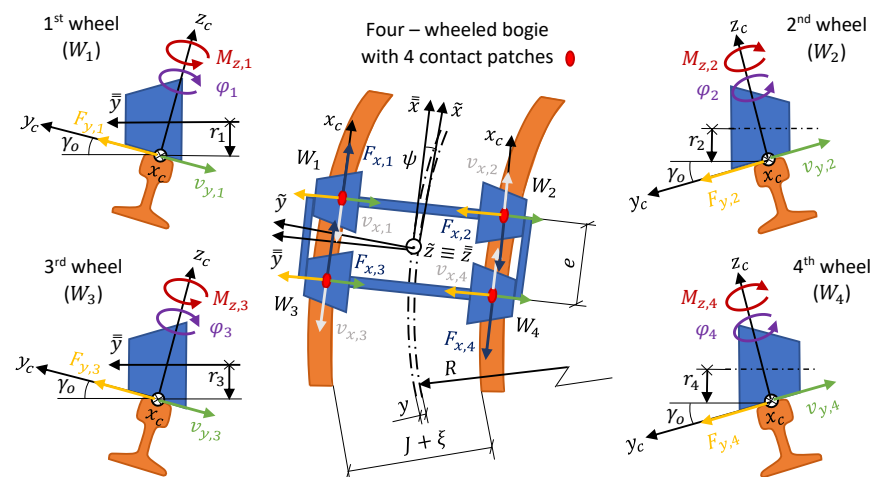
Figure 6. Tangential forces and torques for a four-wheeled bogie. Source: own elaboration.

2.4.4. Calculation of Wear and Prediction of RCF

Wear is the damage to the wheels that reduces their useful life drastically. This wear is due to abrasive and adhesive wear, and models exist based on a wear rate that enables obtaining the wear depth and, hence, characterizing the damage [21]. Abrasive wear is due to the relative movement between the wheel and rail surfaces and their roughness, which causes friction and, in turn, the loss of wheel and rail material. In contrast, adhesive wear is due to plastic deformation and the cohesive forces appearing between both surfaces (Van der Waals, electrostatic or chemical), which ends up producing a material transfer from one surface to the other [20].

For wheel wear characterization, Ref. [20] listed the following hypotheses:

1. The equations are parametrized for abrasive wear and not for adhesive wear, as both phenomena are already included in the resulting wear law if they have been experimentally calibrated.
2. The different mathematical tools study the wear on the wheel profile, where the wear estimated at every instant is cumulative.
3. Wear is assumed to be regular: the variation in the transversal profile is studied, not pattern formation along the longitudinal (circumferential) direction. Thus, the wear at a certain position and instant is extrapolated to the whole circumference.
4. At the contact interface, there are no pollutants. The effect of pollutants is considered by modifying the friction coefficient or introducing new wear laws.

Considering these hypotheses, the models commented upon in Refs. [20,21] can be applied to wheel wear characterization. In Ref. [16], energy transfer models and the RAK model are collected and assessed, and it was determined that the energy transfer using the USFD wear law since its wear law is continuous between wear regimes (mild, severe, catastrophic), so small errors do not lead to great errors in the end.

Moreover, under high axle loads, the stress distribution around the contact patch may cause fatigue cracks on the wheel surface or inside it. For only predicting if RCF is to appear or not, the fatigue index model developed by Ref. [34] and presented in Ref. [21] is useful. The fatigue index (FI_{suf}) is simply the utilized friction term (μ_u) minus the shakedown limit (L_{RCF}), and by comparing its value with zero, 3 situations can be observed: if $FI_{suf} < 0$, RCF is not enough for initiating cracks, while if $FI_{suf} = 0$, this is the limit situation, and cracks are not initiated yet. However, if $FI_{suf} > 0$, RCF initiates cracks on the surface since the tangential force is elevated.

Lastly, Figure 7 shows the wear calculation according to the USFD, which can be eliminated by reprofiling when its depth reaches a certain threshold [19,35,36]. The main equations of the USFD model are displayed thereafter (Equations (41)–(43)), where A_c must be expressed in [mm^2] in Equation (41), while Equation (42) includes the mild, severe and

catastrophic wear regimes, and Equation (43) returns the H_{USFD} value in [μm]) and the main ones of the fatigue index model (Equations (44)–(46)) are shown next:

$$\frac{T\gamma}{A_c} = \frac{|F_x v_x| + |F_y v_y| + |M_z \varphi|}{A_c} \tag{41}$$

$$\begin{cases} W_{R,\,USFD} = 5.3\,\frac{T\gamma}{A_c}, \; for \; \frac{T\gamma}{A_c} \leq 10.4 \\ W_{R,USFD} = 55.0, \; for \; 10.4 < \frac{T\gamma}{A_c} \leq 77.2 \\ W_{R,USFD} = 55.0 + 61.9\left(\frac{T\gamma}{A_c} - 77.2\right), \; for \; \frac{T\gamma}{A_c} > 77.2 \end{cases} \tag{42}$$

$$H_{USFD} = W_{R,USFD}\,\frac{a\,L_{rr}}{\rho \pi r_{rr}} 10^3 \tag{43}$$

$$FI_{surf} = \mu_u - L_{RCF} \tag{44}$$

$$FI_{surf} = \frac{\sqrt{F_x^2 + F_y^2}}{N} - \frac{\tau_{lim}}{p_{z_o}} \tag{45}$$

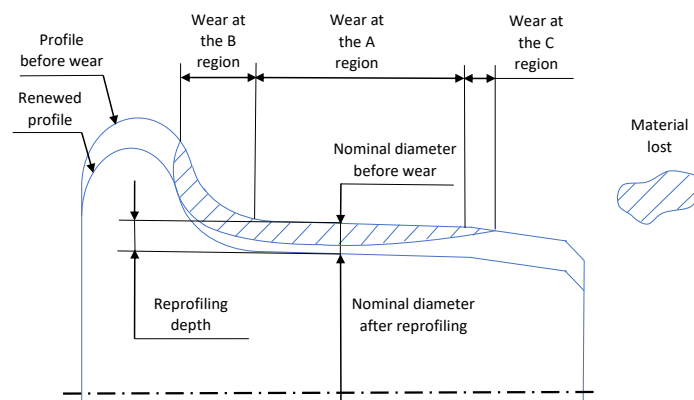$$F_{max,RCF} = \frac{2}{3}\tau_{lim}\pi ab \tag{46}$$

Figure 7. Wheel reprofiling process. Source: own elaboration.

2.5. Software Choice

Once the algorithm has been defined, it must be implemented in an equation-solving program. Due to the large amount of input data, equations, relations, functions, procedures and subroutines that had to be implemented, only software capable of processing the entire volume of data in an agile way was considered. After considering several options (Mathematica, Matlab and Engineering Equation Solver), Engineering Equation Solver [37] was chosen as it allows building algorithms with any architecture based on functions, procedures and subroutines defined in F-Chart programming language, which is a variation of Pascal. The program internally rearranges the equation blocks defined by the user, takes the inputs needed for the new blocks and obtains the requested outputs by means of iterations. These results are obtained after an undetermined number of iterations, depending on adjustable stop criteria such as the relative residuals, which can be as low as 10^{-10} or the limit of iterations. The specific version used is Engineering Equation Solver Professional V9.457-3D (EES). Besides solving algorithms, the chosen program can create parametric tables and graphs derived from those equations.

2.6. Calculation Scenarios

The objective is to perform a sensitivity analysis of the wheelbase and axle load for low-floor wagons so as to study their influence on wear. Prior to obtaining the results,

which are expressed in terms of wheel wear, the calculation scenarios and the input data must be set.

In Ref. [16], many types of bogies are reviewed, and, as it can be seen, those bogies with reduced-diameter wheels need more wheels to take up the same load. This is because reduced-diameter wheels can withstand lower axle loads than ordinary-diameter wheels (obviously, smaller wheels have less material), so more wheels are needed for the same bogie load. Also, the minimum diameter after the reprofiling cycles is more restrictive in reduced-diameter wheels for operating safety reasons.

For the sensitivity analysis, these two commercial bogies, used or proposed on rail motorways, were chosen:

- Y25: This bogie consists of four wheels (thus, it is composed of two wheelsets), and it can take up 45 t in total (22.5 t/axle) at a maximum speed of 120 km/h. The nominal wheelbase (e) is 1.800 m, and the wheels are braked, in general, by brake shoes. The wheel nominal diameter (D) ranges from 920 mm (original, maximum) to 840 mm (operational minimum).
- Graz Pauker 702: This bogie is composed of eight wheels (so four wheelsets), and it can withstand 20 t (5 t/axle) at 100 km/h. The nominal total wheelbase (e) is 2.700 m (1 + 0.700 + 1 m are the nominal partial wheelbases (e')), and the wheel nominal diameter (D) ranges from 355 to 335 mm.

The sensitivity analysis was performed for both bogies, for which four calculation scenarios were established for each (eight scenarios in total, ranging from (a) to (h)). The values chosen for each and every scenario are presented in Table 1:

Table 1. Specific input values for each of the eight scenarios.

Variable	D (m)	n_{ejes} (∅)	r_p (m)	e (m)	λ_{eje} (kg)
(a)	0.920	2	0.467–0.475	1.800	13,750
(b)	0.920	2	0.467–0.475	1.800	22,500
(c)	0.920	2	0.467–0.475	1.020	18,784
(d)	0.920	2	0.467–0.475	2.540	18,784
(e)	0.355	4	0.185–0.193	1.800	3750
(f)	0.355	4	0.185–0.193	1.800	5000
(g)	0.355	4	0.185–0.193	1.365	6996
(h)	0.355	4	0.185–0.193	2.540	6996

Regarding the choice of these values, the following must be noted:

1. The flange radius (r_p) is obtained as the addition of the nominal rolling radius (r_0, half of D) and a constant.
2. The total wheelbase (e) values must be within $\left[(D + 100) \cdot \left(n'_{ejes} - 1 \right) ; 2.700 \right]$, since ensuring that minimum avoids wheel interference and that maximum avoids restricted movement (less than 1% of the tightest curve radius, as explained in Section 2.7).
3. The axle load values of 18,784 kg for 920 mm diameter wheels and 6996 kg for 355 mm wheels are equivalent in relation to the material quantity. Specifically, both values generate a 1235 MPa normal pressure, which is a mean pressure value (maximum axle loads usually induce 1100–1300 MPa on the wheel), even if the load value for the smaller wheel surpasses the manufacturer's limit. Further details are given in Ref. [16].

The rest of the conditions are the same (for instance, the rail radii) and are discussed in Section 2.7. Only realistic, feasible and plausible values were set, and even variations in the geometry and friction were considered (the variation in dry friction with speed).

Taking all of this into account, the eight scenarios were established: Scenario (a)–Scenario (h). For each of them, the input data were first entered, and then the program ran the algorithm for every stretch of the railway line, switching the direction when the end station was reached. When the wear depth reached a certain threshold, then the wheel was

reprofiled, and the scenario execution started over with a new wheel profile (with a lesser diameter now). After a certain number of reprofiling cycles was reached, the minimum allowed diameter was reached, and the scenario execution ended. All of this is registered in the wheel diameter–mileage curves, which are presented in Section 3.

Regarding the wear depth threshold, this must be as low as possible, for the wheel profiles are not updated as they wear out, so they must be renewed frequently. A sensible value is 1 mm for the three scenarios (this is not an input value but rather a stop criterion). The lathe have to be removed a bit more for the right reprofiling: 1.5 mm. By converting these radial data into diametral data, 2 and 3 mm are obtained.

Finally, Figure 8 illustrates the placement of the $\overline{uvw}$ reference frame for the bogies (this reference frame is necessary for the center of friction model), the wheels entering a curve first are shown (wheels W_1 and W_2 lead half of the time and trail the other half), and the wheel and rail profiles are geometrically adjusted, also paying attention to the flange–rail contact:

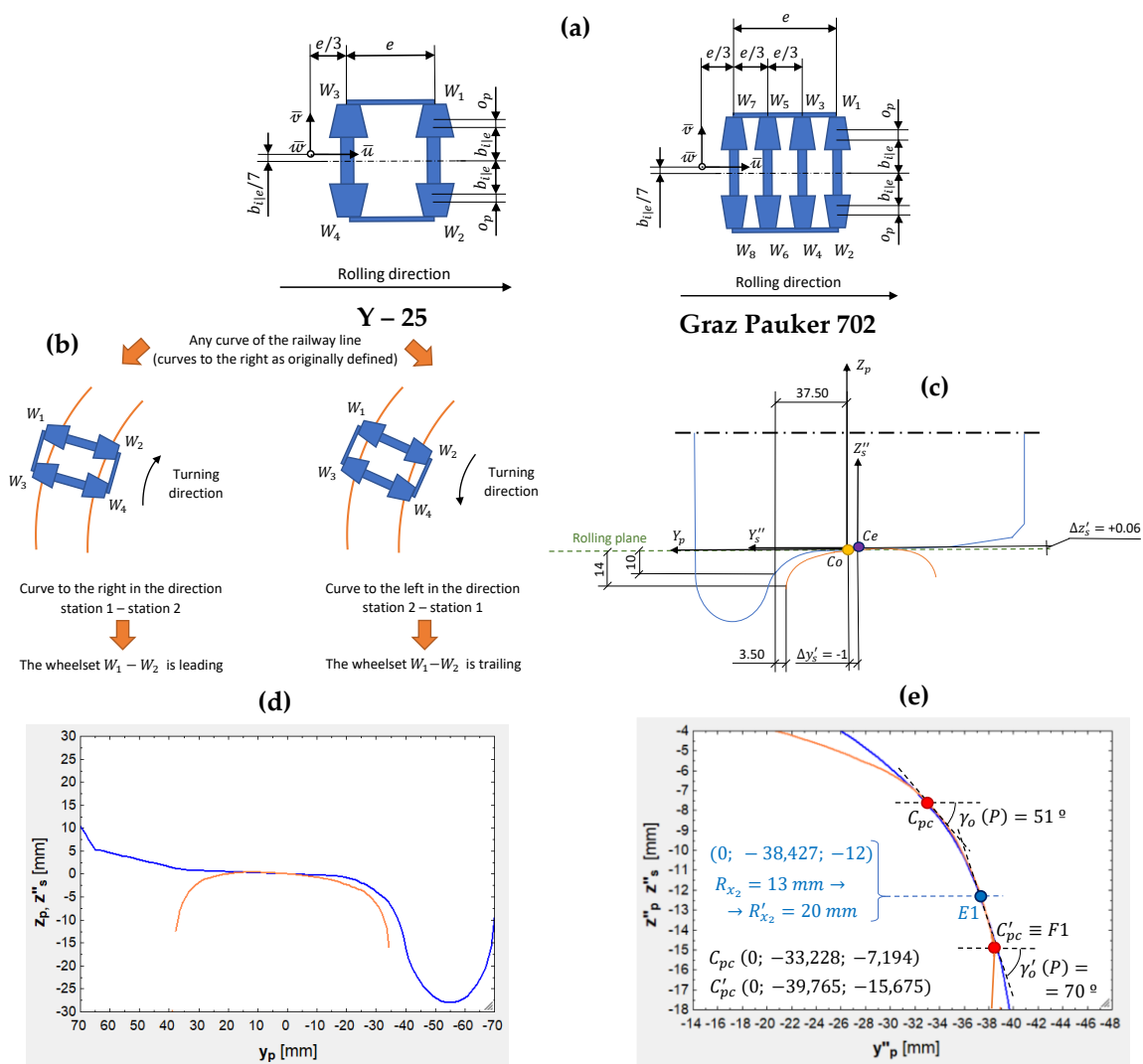**Figure 8.** (**a**) Placement of the $\overline{uvw}$ reference frame for the bogies considered; (**b**) position of the wheelsets according to the curve direction; (**c**) relative positioning of the right wheel and rail at straight sections; (**d**) relative positioning of the left wheel and rail at straight sections; (**e**) adjustment between the left flange and rail for wear distribution. Source: own elaboration.

2.7. Input Data

As can be seen in Figure 3, information about the vehicle and the infrastructure needs to be input into the algorithm before it is run. The vehicle speed can be linked to the railway line definition if it runs at the maximum allowed speed at the infrastructure.

For the eight scenarios, the wheel profile portrays the geometry of the 1/40 standard profile and is made from the state-of-the-art and lower-wearing (for freight trains) ER8 steel grade, while the rail profile portrays the geometry of the 60E1 standard profile and is made from R260 steel grade, also state-of-the-art and lower-wearing (for freight lines) [22]. Most of the wheelset and bogie characteristics, which are taken from the bogie comparison carried out in Ref. [16], are also common to the three scenarios. The same is true for the parameters used to modify the friction with speed according to Polach's method (implemented with variable friction under dry conditions). These common input data are shown in Table A3 (Appendix C).

Regarding the railway line parameters, the calculation was performed for the three scenarios with data from a non-existing railway line. The design parameters of a railway line are defined in Refs. [23,38], although not all of the parameters were used for wear calculation.

In Ref. [16], a railway line is defined stretch by stretch, with the following parameters:

- Initial and final metric points (Q_{in} and Q_f, respectively).
- Type of stretch: RECTA (straight), CIR (circular curve), CLO (clothoid), PARACUAD (quadratic parabola) or PARACUB (cubic parabola).
- Direction of the curve: NING (the stretch is straight), IZDA (curve to the left) or DCHA (curve to the right).
- Position of the bogie at the curve: NING (the stretch is straight), ENT (the bogie is entering the curve), SAL (the bogie is exiting the curve).
- Curve radius (R), cant (h_r) and inclination (i).
- Initial and final maximum speed allowed (V_{in} and V_{fn}, respectively).

Constant values as the track gauge (1.668 m) are the same for all of the stretches, and the gauge widening is a piecewise-defined function that can be directly imported from Ref. [23], which specifies the gauge widening parameter (ξ) as a function of the curve radius (R). For example, ξ is null for curves with R greater than 300 m, and ξ is equal to 20 mm for curves with R between 100 and 150 m. Other values, such as the transition curves parameters, are pre-defined, and others can be inferred through equations. For instance, the distance traveled between two metric points is their difference.

The 333 stretches defined in Ref. [16] can be found in the Supplementary Materials. The curve radii range from a minimum of 265 m (the ratio e/R_{min} is less than 0.01, and according to this heuristic rule, any restricted movements will not appear) to a maximum tending to infinity at straight sections (∞ is not accepted on EES, so it is assimilated to 5×10^7), with 200–800 m radii as the most frequent. For more realism, station 1 is called Albarque, station 2 is called Zacarín, and there is even an intermediate station called Milbello (all of these are fictional names).

Finally, it is noteworthy that the attached material also includes the polynomial fittings of Hertz's and Kalker's coefficients, as well as other equations (displayed as part of the algorithm already) [39].

3. Results

3.1. Scenarios for 920 mm Wheels, from (a) to (d)

After executing the algorithm, the diameter–mileage curves are obtained. Here, the diameter is expressed in [mm], whereas the distance traveled is in [km]. The results are discussed in the Section 4, but some numbers can be anticipated:

1. When the 920 mm wheels are mounted on a bogie with e = 1.800 m and λ_{eje} = 13,750 kg, they can travel for 159,110 km until reaching an 840 mm diameter, losing 2 mm

in diameter at every reprofiling cycle. At that point, the worn-out profile will be discarded for safety and operational reasons.

2. When the 920 mm wheels are mounted on a bogie with $e = 1.800$ m and $\lambda_{eje} = 22,500$ kg, they can travel for 106,007 km until reaching an 840 mm diameter, losing 2 mm in diameter at every reprofiling cycle. At that point, the worn-out profile will be discarded for safety and operational reasons.

3. If, instead, the 920 mm wheels are assembled on a bogie with $e = 1.020$ m and $\lambda_{eje} = 18,784$ kg, they can travel for 145,278 km until reaching an 840 mm diameter.

4. Lastly, if the 920 mm wheels are on a bogie with $e = 2.540$ m and $\lambda_{eje} = 18,784$ kg, they can travel for 90,194 km until reaching an 840 mm diameter.

Figure 9 displays the four diameter–mileage curves. They were plotted using the same scales on both axes for the sake of visual comparison. As can be seen, the wheel always starts with a 920 mm nominal diameter (at the tread). Right after reaching the wear depth limit (1 mm in radius or 2 mm in diameter, reached at the flange first), the wheel is sent to the workshop for lathing. This process starts with a diameter close to 920 mm at the tread (barely worn-out) and ends with a 917 mm diameter at the tread. Therefore, 3 mm material is removed (1.5 mm in radius, at each side if looked on a cross-section). The wheel exits the workshop with a 917 mm diameter, and it wears out until 915 mm, then it is reprofiled from 917 to 914 mm, and so on.

Figure 9. (**a**) Diameter–mileage curve for the 920 mm diameter wheel with $e = 1.800$ m and $\lambda_{eje} = 13,750$ kg; (**b**) results for the same wheel, but with $e = 1.800$ m and $\lambda_{eje} = 22,500$ kg; (**c**) results for the same wheel, but with $e = 1.020$ m and $\lambda_{eje} = 18,784$ kg; (**d**) results for the same wheel, but with $e = 2.540$ m and $\lambda_{eje} = 18,784$ kg.

3.2. Scenarios for 355 mm Wheels, from (e) to (h)

After executing the algorithm, the diameter–mileage curves are obtained. Here, the diameter is expressed in [mm], whereas the distance traveled is in [km]. The results are discussed in the Section 4, but some numbers can be anticipated:

1. When the 355 mm wheels are mounted on a bogie with e = 1.800 m and λ_{eje} = 3750 kg, they are able to travel for 49,359 km until reaching their minimum allowed diameter: 335 mm. This is the real-life end for this wheel, yet the wear–reprofiling cycles are extended as if the final diameter could be 275 mm since the difference between 355 and 275 is the same as that of 920 and 840. In this fictional situation, the wheel would have traveled 180,414 (fictional-life end).

2. When the 355 mm wheels are mounted on a bogie with e = 1.800 m and λ_{eje} = 5000 kg, they are capable of traveling 38,434 km until reaching their minimum allowed diameter of 335 mm. This is the real-life end for this wheel, yet the wear–reprofiling cycles are extended as if the final diameter could be 275 mm since the difference between 355 and 275 is the same as that of 920 and 840. In this fictional situation, the wheel would have traveled 140,481 km (fictional-life end).

3. If, instead, the 355 mm wheels are assembled on a bogie with e = 1.020 m and λ_{eje} = 5000 kg, then they are capable of traveling 36,483 km until reaching their minimum allowed diameter of 335 mm. In this scenario, the life end could fictionally be 133,352 km (fictional-life end).

4. Lastly, if the 355 mm wheels are on a bogie with e = 2.540 m and λ_{eje} = 6996 kg capable of traveling 21,011 km until reaching their minimum allowed diameter of 335 mm. In this scenario, the life end could fictionally be 76,795 km (fictional-life end).

Figure 10 displays the four diameter–mileage curves. They were plotted using the same scales on both axes for the sake of visual comparison. As can be seen, the wheel always starts with a 355 mm nominal diameter. Right after reaching the wear depth limit (1 mm in radius or 2 mm in diameter), the wheel is lathed. This process starts with a diameter close to 355 mm at the tread and ends with a 352 mm diameter at the tread. Therefore, 3 mm material is removed. The wheel exits the workshop with a 352 mm diameter, and it wears out until 350 mm, so then it is reprofiled from 352 to 349 mm, and so on.
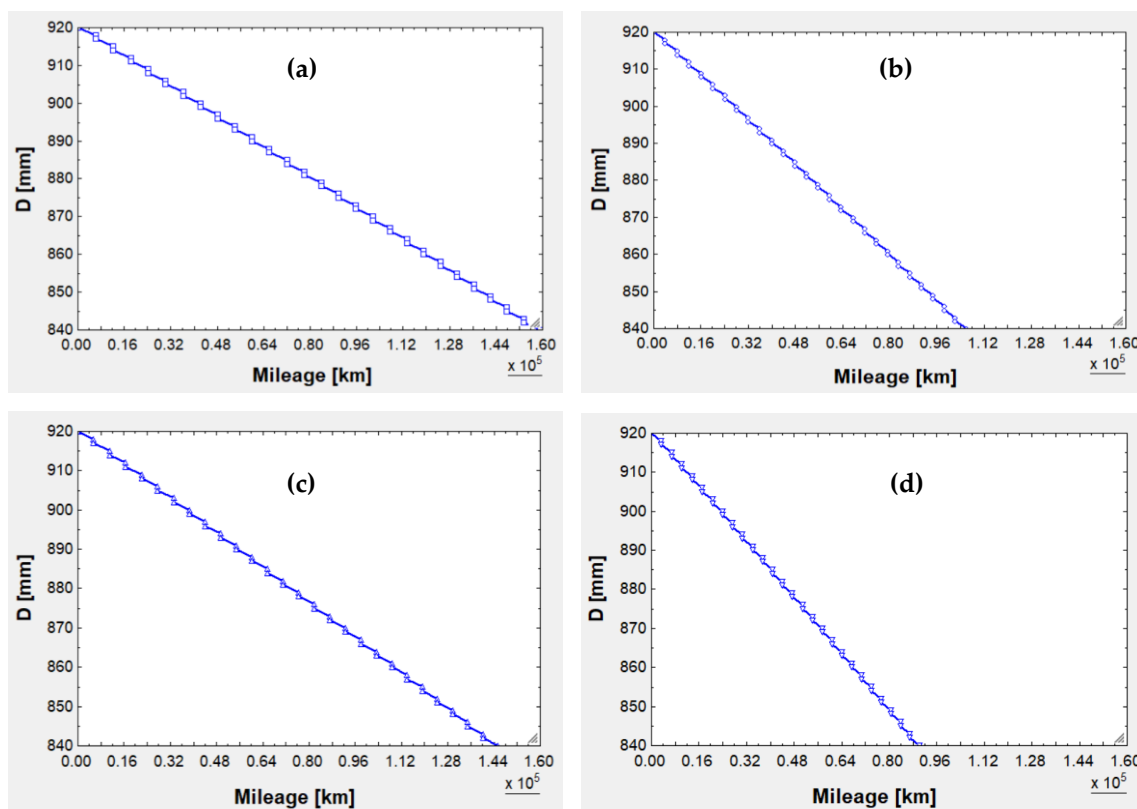

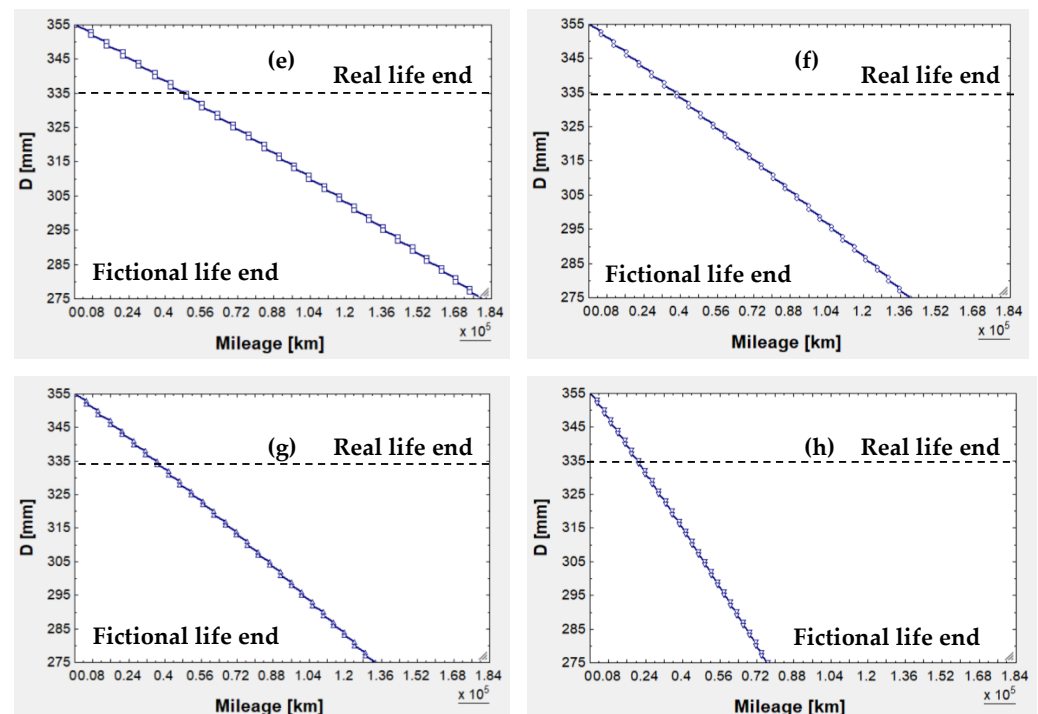**Figure 10.** (**e**) Diameter–mileage curve for the 355 mm diameter wheel with e = 1.800 m and λ_{eje} = 3750 kg; (**f**) results for the same wheel, but with e = 1.800 m and λ_{eje} = 5000 kg; (**g**) results for the same wheel, but with e = 1.365 m and λ_{eje} = 6996 kg; (**h**) results for the same wheel, but with e = 2.540 m and λ_{eje} = 6996 kg.

4. Discussion

A model capable of calculating wheel wear is presented in this work, and it was used to perform a sensitivity analysis of varying influential factors on wear, such as wheelbase and axle load. For the understanding of these results and the observation of trends, it is necessary to review certain aspects found when analyzing all of the work overall, also delving into the underlying equation blocks which eventually lead to the diameter–mileage curves:

- Scenarios from (a) to (d) can be compared to the life of a 920 mm wheel with e = 1.800 m and λ_{eje} = 18,874 kg: 124,275 km, computed in Ref. [16].
- The 920 mm wheel can operate for 159,110 km in scenario (a), which implies a 28.03% increase; for 106,007 km in scenario (b), implying a 14.70% decrease; for 145,278 km in scenario (c), yielding a 16.90% increase; and, finally, for 90,194 km in scenario (d), a 27.42% decrease.
- Scenarios from (e) to (h) can be compared to the life of a 355 mm wheel with e = 1.800 m and λ_{eje} = 6996 kg: 26,985 km (real-life end) and 101,433 km (fictional-life end), calculated in Ref. [16].
- Regarding real-life ends, the 355 mm wheel can operate for 49,359 km in scenario (e), which implies an 82.91% increase; for 38,434 km in scenario (f), implying a 42.43% increase; for 36,483 km in scenario (g), yielding a 35.20% increase; and, finally, for 21,011 km in scenario (h), a 22.14% decrease.
- Regarding fictional-life ends, the 355 mm wheel can run for 180,414 km in scenario (e), which implies a 77.87% increase; for 140,481 km in scenario (f), implying a 38.50% increase; for 133,352 km in scenario (g), yielding a 31.47% increase; and, finally, for 76,795 km in scenario (h), a 24.29% decrease.
- These trends are plotted in Figure 11. The scenarios associated with axle load variation ((a), (b), (e) and (f)) are shown in Figure 11a, while those associated with wheelbase variation (c), (d), (g) and (h)) are in Figure 11b:
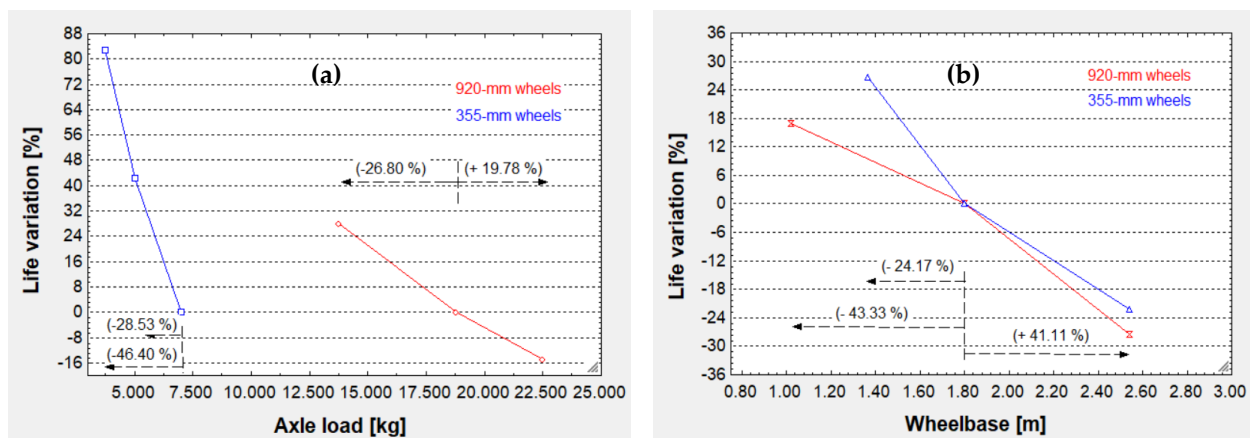
Figure 11. (**a**) Life variation with axle load for 920 and 355 mm wheels; (**b**) life variation with wheelbase for the same wheels.

- As it can be seen, increasing axle load is worse than increasing wheelbase (which has an enormous percentual increase). This is because increases in axle load augment both wear depth and the width of the contact patch, whereas increases in wheelbase only augment the former.
- The distance difference between reprofiling (the reprofiling span) is very variable. Should the wagons perform n routes Albarque–Zacarín–Albarque (75.272 km) a week, then reprofiling periodicity should be Reprofiling span · (7/(75.272n)). Because the reprofiling span is not constant inside any of the scenarios, the mean value must be computed for everyone.

- According to the reprofiling periodicity criterion, some scenarios are much more unfavorable than others. Scenario (h) has a mean reprofiling span below 3000 km, while in scenario (e), more than 6500 km are reached. The next bar plot, in Figure 12, displays this information.

Figure 12. Mean reprofiling span for each scenario.
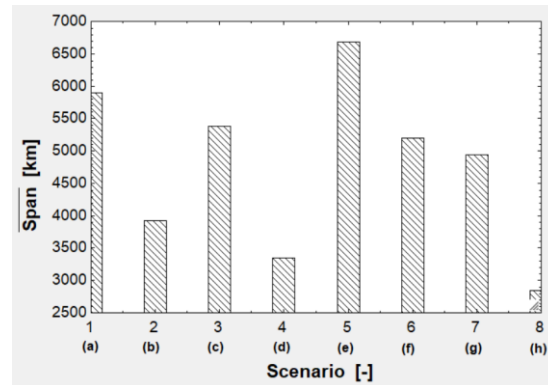
- From a maintenance economy perspective, scenarios (a), (c), (e), (f) and (g) are preferable because the wheels go to the workshop less often and live longer, so they also have to be replaced less frequently.
- RCF is predicted for every flange–rail contact as normally $F_{surf} > 0$ in these situations (except for isolated cases where the 355 mm wheel is negotiating curves with radii close to the threshold radius) as a consequence of the high normal pressure ($P_{z_o} = 5 - 7$ GPa) at the flange contact area with the rail, which stacks up hydrostatically over a tiny contact area. All of this leads to a high wear index ($T\gamma/A_c$), which falls in the severe region of the USFD wear law.
- It is interesting to gather some intermediate results showing the extent of RCF on one 920 mm wheel with e = 1.800 m and λ_{eje} = 18,874 kg, and one 355 mm wheel with e = 1.800 m and λ_{eje} = 699 kg, which negotiates the tightest curve belonging to the line layout; that is, R = 265 m, so flange–rail contact occurs. These intermediate results are shown in Table A4 (Appendix D).
- As it can be seen, $FI_{surf}(355) = 0.409 < FI_{surf} = 0.433$; $p_{z_o}(355) = 6584 \times 10^9 > p_{z_o}(920) = 6.401 \times 10^9$ Pa; $T\gamma(355) = 367.887 < T\gamma(920) = 468.088$ N; $A_c(355) = 17.36 < A_c(920) = 20.03$ mm^2; $T\gamma/A_c(355) = 21.192 < T\gamma/A_c(920) = 23.368 \frac{N}{mm^2}$; $W_{R,\ USFD}(355) = W_{R,\ USFD}(920) = 55 \frac{\mu g}{m \cdot mm^2}$; $H_{USFD}(355) = 3.538 > H_{USFD}(920) = 2.295$.
- So, except for the normal pressure and the wear depth, the rest of the values are less for reduced-diameter wheels, where RCF is less intense. The normal pressure increases because the contact is smaller, whereas the wear depth increases (despite being the wear rate the same and typical of the severe wear regime) because the reduced-diameter wheel must turn more times (the number of revolutions is higher) to travel the same linear distance as the ordinary-diameter one.
- Another appreciation from Table A4 is that flange–rail contact is slightly more benign for reduced-diameter wheels; thus, the forces are less intense: $F_x(355) = 1009 < F_x(920) = 1274$ N; $F_y(355) = 34,760 < F_y(920) = 41,159$ N; $M_z(355) = 55.280 < M_z(920) = 197.200$ N · m. Regarding the normal force on the flange, the same trend is observed: $N(355) = 76,224 < N(920) = 85,465$ N.
- Not only are dynamics more benign, but kinematics are also smoother. By applying Redtenbacher's formula to both wheels, as in Figure 13a, and the total uncentering equation, as in Figure 13b, it can be seen that reduced-diameter wheels tend to uncenter less than ordinary-diameter ones, so they can negotiate curves more smoothly, even in the worst case (leading wheelset and outer wheel):
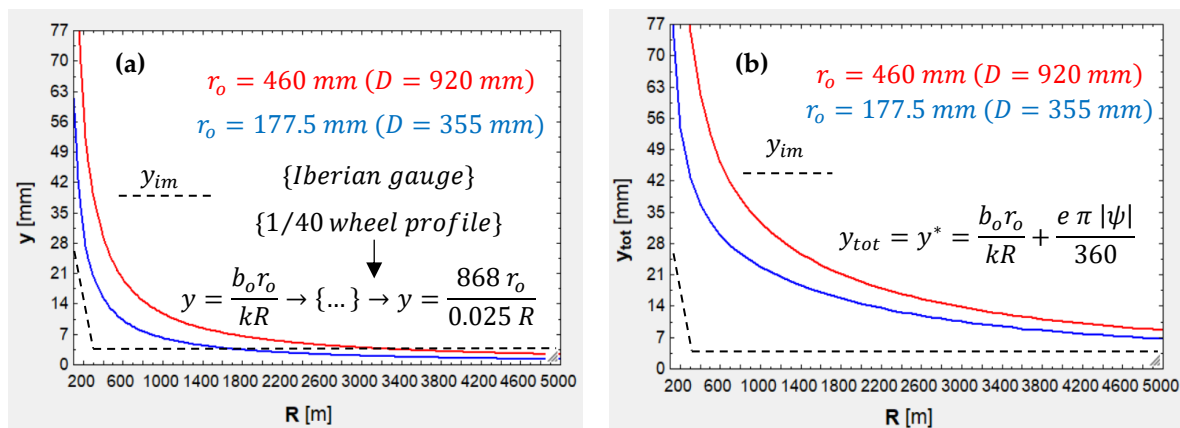
Figure 13. (**a**) Partial uncentering for different r_o and R values; (**b**) total uncentering for the same values.

5. Conclusions

A sensitivity analysis was carried out, and some trends were observed, all of which were compared regarding wheel wear, which is a physical problem affecting the railway maintenance economy and has been tackled through mathematical modeling.

The algorithm constructed interconnects some calculation models and methods by other authors, all of which exhibit good accuracy–computational effort ratios. Moreover, it allows for taking into account the main factors impacting wheel wear, some of which are associated with the vehicle (wheel and wagon factors), while others are associated with the superstructure. By introducing boundary conditions and hypotheses complementing those of the calculation models used, the algorithm enables computing the wear with a parametric variation (diameter variation, among others).

In the case presented, wheel wear computations were utilized to obtain diameter–mileage curves for eight scenarios. The main conclusions extracted are as follows:

1. Varying axle load has a more acute effect than varying the wheelbase, which can be explained theoretically: increases in axle load augment both wear depth and the width of the contact patch, whereas increases in wheelbase only augment the former.
2. Reduced-diameter wheels live shorter than ordinary-diameter ones as they cannot go through the same number of reprofiling cycles due to the manufacturers' and operators' limitations, which are imposed since a wheel that has lost a big percentage of its volume cannot withstand the same load and suffers RCF more intensely.
3. Even if they could, reduced-diameter wheels would still live shorter due to their greater angular contact with the rail (number of revolutions), which increases the wear depth at most of the curves. However, this effect is non-linear, as kinematics and dynamics are slightly more benign for reduced-diameter wheels.
4. That means that halving the diameter does not imply halving the wheel lifespan, as the lifespan reduction is less than half.
5. RCF is predicted for every flange–rail contact, so adopting mitigation strategies is necessary.

In light of these conclusions, several recommendations for the rail motorway industry (the carriers) may be provided:

(a) Regarding maintenance economy, reduced-diameter wheels go to the workshop more often, but they can go through fewer reprofiling cycles than ordinary-diameter ones, so the reduced-diameter wheels must be replaced more often. Additionally, the double wheels must be reprofiled at every cycle. This implies that the maintenance cost for reduced-diameter wheels is, presumably, higher.

(b) Even a Graz Pauker bogie loaded at 7 t/axle with a wheelbase below or equal to 1.800 m cannot beat a Y25 bogie loaded at 18.5 t/axle or up to 22.5 t/axle and a wheelbase below or equal to 1.800 m. The former can only take up 28 t (56 t the whole wagon), while the latter, 37 t or up to 45 t (74–90 t the whole wagon).

(c) Y25 bogies with their 920 mm wheels are the best option unless extensive work would be required to increase the loading gauge at tunnels and overpasses. In that case, an economical study should be performed that could lead to the usage of Graz Pauker 702 bogies with 355 mm wheels.

(d) It must also be noted that wagons equipped with Y25 wagons are more difficult to load due to their shape, and the articulated vehicle's cabin does not usually fit on the wagon.

(e) The wheels of Y25 bogies live longer when they do not reach their maximum axle load (22.5 t/axle). Also, when the wheelbase is below 1.800 m, a realistic wheelbase value should consider the strength of the bogie beams and the room taken up by the suspension stages.

(f) The load inside the heavy articulated vehicles should be appropriately distributed. Advanced weighing techniques must ensure that axle loads hold mostly constant and do not vary abruptly (for instance, one wheelset loaded with 8 t and the next one with 22.5 t). This uniformity allows for more even wear on the bogie or both bogies of a wagon.

Finally, as a continuation of this research work, a list with the following steps to be carried out is presented:

- Consideration of uncentered (respecting the ± 10 mm tolerance [1] and uneven axle load across the wheelsets).
- Variation in less influential factors (H_{CdG}, for instance) in order to develop sensitivity analyses with the goal of tune-fining.
- Variation in the track gauge in order to consider the effect of track gauge on wheel wear.
- Reformulation of the algorithm in order to mesh the contact patch and execute calculations globally, including all of the elastic microslips.
- Consideration of conformal contacts, also by means of finite elements, as it is not possible to apply Hertz's solution to this type of contact.
- Addition of rail wear, which would have an impact on wheel wear, as the rail curvatures would change (favorably, in general) and the contact positions would differ.
- Updating the contact parameters immediately after the wheel starts to wear out. This would allow for the computation of the actual semi-conicity, contact angle and radii.
- Inclusion of the wheel and rail surface roughness, which would require powerful software able to characterize surfaces with a micrometric resolution.
- Consideration of a different friction coefficient for the tread and flange, as it is not always the same, as well as other weather conditions and flange lubrication.
- Study of the effect of brake shoes on the tread. The shoes would tend to increase the tread wheel, yet the overall effect is not very pronounced (the shoes wear out first). The shoes are also helpful for wiping pollutants off of the wheels (for example, leaves).
- Optimization of the maximum wear depth taking into account economic factors: often, reprofiling would lower derailment and crack-failure risks; however, that would come at a high cost, so the trade-off point should be optimized.
- Comparison of the theoretical data with those obtained by simulation with tools specialized in railway dynamics (ADAMS/rail, for instance, which would enable a multibody dynamics simulation).
- Conduction of experiments in order to collect real data and compare it to the theoretical data. Analyzing data from a truck operation, including axle loads, speeds, trajectories and wheel wear, would be crucial. For that, sensors and monitoring systems on the tracks so as to monitor the dynamic responses of the wagons would be suitable.

Appendix A

Table A1. Latin symbol abbreviations.

Abbreviation	Definition	Unit (SI)	Abbreviation	Definition	Unit (SI)
a	Longitudinal semi-axis of Hertz's ellipse	m	n_{dec}	Degree of the function deceleration–time	Ø
a_{lat}	Lateral acceleration experienced by the vehicle	$m \cdot s^{-2}$	n_{ejes}	Number of axles on the vehicle	Ø
A	Relative longitudinal curvature	m^{-1}	n'_{ejes}	Number of axles on the bogie	Ø
A_c	Hertz's ellipse area	m^2	n_H	Lateral Hertz's coefficient	Ø
A_f	Ratio between the minimum friction coefficient (infinite slip speed) and the maximum (null slip)	Ø	N	Reaction force of the rail on the wheel on the normal contact direction (normal force)	N
b	Lateral semi-axis of Hertz's ellipse	m	$N_{br} \vert N_p$	Reaction force of the rail on the wheel in the normal direction to the contact area at the (tread flange) at a wheel experiencing flange–rail contact	N
$b_i \vert b_e$	Distance from track center to the rolling radius of the (inner ǀ outer) wheel in relation to the curve	m	$N_e \vert N_i$	Normal force acting on the (outer ǀ inner) wheel in relation to the curve	N
b_o	Distance from track center to rolling radius	m	$N_r \vert N_t$	Normal force component in the radial ǀ tangential direction (the tangential one is perpendicular to the radial one)	N
B	Relative lateral curvature	m^{-1}	$N_\perp \vert N_\parallel$	Normal force component acting on the wheel (perpendicularly ǀ tangentially) to contact area	N

Table A1. *Cont.*

Abbreviation	Definition	Unit (SI)	Abbreviation	Definition	Unit (SI)
B_f	Exponential constant at friction law	$\text{s} \cdot \text{m}^{-1}$	o	Existing offset between the track gauge minus the flange–rail play and the distance between the nominal radius center of the wheelset wheels	m
c	Effective size of contact patch	m	o_p	Horizontal distance between the center of the flange contact area center and the center of the wheel	m
C	Contact tangential stiffness	$\text{N} \cdot \text{m}^{-3}$	p_{z_o}	Maximum contact normal pressure	Pa
C_S	Contact tangential stiffness for the pure spin case	$\text{N} \cdot \text{m}^{-3}$	$Q_i \| Q_f$	Initial | final metric point	m
$C_{11} \| C_{22} \| C_{33}$	Longitudinal | lateral | vertical Kalker's coefficient	Ø	$r_e \| r_i$	Theorical rolling radius of the (outer | inner) wheel in relation to the curve	m
$C'_{11} \| C'_{22}$	Kalker's coefficient (longitudinal | lateral) corrected according to non-dimensional slip components	Ø	$r_e^* \| r_i^*$	Rolling radius of the (outer | inner) wheel in relation to the curve, including the displacement due to the yaw angle	m
$C_{23} \| C_{32}$	Kalker's coefficients on $y_c z_c$ plane	Ø	r_o	Nominal rolling radius	m
D	Nominal wheel diameter	m	r_p	Wheel radius measured until the flange contact patch	m
e	Total bogie wheelbase (measured from its leading to trailing wheelset)	m	r_{rr}	Real rolling radius	m
e'	Partial bogie wheelbase (measured between 2 next wheelsets)	m	r_H	Vertical Hertz's coefficient	Ø
E	Equivalent Young's modulus of the materials in contact	Pa	R	Curve radius (measured from its center to the track axis)	m
$E_1 \| E_2$	Young's modulus of the rail | wheel	Pa	R_{x1}	Rail lateral radius	m
f_i	Sagitta of the inner rail in relation to the curve	m	R_{x2}	Wheel lateral radius	m
F	Magnitude of tangential force vector	N	R_{y1}	Rail longitudinal radius	m
F_f	Braking force	N	R_{y2}	Longitudinal wheel radius	m
F_t	Traction force	N	s	Magnitude of non-dimensional slip vector	Ø

Table A1. *Cont.*

Abbreviation	Definition	Unit (SI)	Abbreviation	Definition	Unit (SI)
$F_x\vert F_y$	Longitudinal | lateral tangential force	N	$s_x\vert s_y$	Longitudinal | lateral non-dimensional slip	Ø
$F_x'\vert F_y'$	Longitudinal | lateral tangential force translated to the reference frame $\overline{u}\,\overline{v}\,\overline{w}$	N	s_C	Magnitude of non-dimensional slip corrected with the spin contribution	Ø
$F_{y,C}$	Lateral tangential force (lateral force) corrected with the spin contribution	N	$s_{y,C}$	Lateral non-dimensional slip corrected with the spin contribution	Ø
$F_{y,S}$	Increase in lateral force due to spin	N	$T\gamma/A_c$	Wear index for the USFD law	$\text{N}\cdot\text{m}^{-2}$
$F_{mx,RCF}$	Maximum tangential force before rolling contact fatigue appears	N	u_f	Coordinate in the $\overline{u}$ axis of the wheel contact area, in the reference frame $\overline{u}\,\overline{v}\,\overline{w}$	m
FI_{surf}	Fatigue index	Ø	u_{fl}	Coordinate in the $\overline{u}$ axis of the flange outer part, in the frame $\overline{u}\,\overline{v}\,\overline{w}$	m
g	Gravity acceleration	$\text{m}\cdot\text{s}^{-2}$	v_f	Coordinate in the $\overline{v}$ axis of the wheel contact area, in the frame $\overline{u}\,\overline{v}\,\overline{w}$	m
G	Equivalent shear modulus of the materials in contact	Pa	v_{fl}	Coordinate in the $\overline{v}$ axis of the flange outer part, in the frame $\overline{u}\,\overline{v}\,\overline{w}$	m
$G_1\vert G_2$	Shear module of the rail | wheel	Pa	$v_x\vert v_y$	Longitudinal | lateral creepage	Ø
h_r	Real cant of the railway line	m	V	Vehicle speed	$\text{m}\cdot\text{s}^{-1}$
H_{CdG}	Center of gravity of λ_{eje} height over the rolling plane		$V_f\vert V_i$	Final | initial vehicle speed	$\text{m}\cdot\text{s}^{-1}$
H_{tara}	Center of gravity of λ_{tara} height over the rolling plane	m	$w_x\vert w_y$	Longitudinal | lateral slip speed	$\text{m}\cdot\text{s}^{-1}$
H_u	Center of gravity of λ_u height over the rolling plane	m	w_w	Wheel width	m
H_{USFD}	Total wheel wear depth (USFD law)	m	$W_{R,USFD}$	Wear rate (USFD law)	$\text{kg}\cdot\text{m}^{-1}\cdot\text{m}^{-2}$
i	Railway line gradient/slope	m	y	Wheelset uncentering	m
J	Track gauge	‰	y^*	Total wheelset uncentering	m
k	Wheel semi-conicity or inclination	m	y_{lm}^*	Available play for the bogie leading wheelset when it uncenters towards the outside of a curve	m

Table A2. Greek-symbol abbreviations.

Abbreviation	Definition	Unit (SI)	Abbreviation	Definition	Unit (SI)
$k_A \| k_S$	Reduction coefficient for the initial slope of the traction curve at the stick|slip region	Ø	$y^*_{lm,diag}$	Available play for the bogie trailing wheelset when it uncenters towards the inside of a curve	m
K_M	Auxiliary coefficient for the calculation of $F_{y,s}$	Ø	$\dot{y}$	Wheelset uncentering rate	$\text{m} \cdot \text{s}^{-1}$
L_{rr}	Length really rolled by a wheel	N	$\dot{y}^*$	Total wheelset uncentering rate	$\text{m} \cdot \text{s}^{-1}$
m_H	Longitudinal Hertz's coefficient	m	Z_w	Number of wheels on the bogie	Ø
M_Z	Spin torque	$\text{N} \cdot \text{m}$			
α_{fn}	Fraction of the force normal to the wheel falling on the flange contact patch	Ø	μ_o	Initial friction coefficient or maximum (null slip speed)	Ø
β_{rp}	Gradient angle	rad	v	Equivalent Poisson's ratio of the materials in contact	Ø
γ_o	Wheel contact angle	rad	$v_1 \| v_2$	Poisson's ratio of the rail|wheel	Ø
δ_o	Maximum indentation between the two bodies in contact	m	ξ	Gauge widening (at tight curves)	m
δ_P	Auxiliary coefficient for the obtention of coefficient K_M	Ø	ρ	Density of the wheel material	$\text{kg} \cdot \text{m}^{-3}$
ε	Tangential stress gradient at the stick region	Ø	ς	Longitudinal displacement angle of the contact patch	rad
ε_S	Tangential stress gradient at the stick region for the pure spin case	Ø	τ_{mx}	Maximum tangential stress transmitted	Pa
$\zeta_h \| \zeta_v$	Load (horizontal|vertical) on the flange contact patch	N	τ_{lm}	Tangential yield stress of the wheel material	Pa
η	Play between the flange and the rail	m	η	Tilt angle	rad
θ	Hertz's angle	rad	$\dot{\Phi}$	Variation angle of tilt angle	$\text{rad} \cdot \text{s}^{-1}$
ϑ_r	Real cant angle	rad	φ	Spin (rotational creepage)	$\text{rad} \cdot \text{m}^{-1}$
λ_{eje}	Axle load	kg	ψ	Yaw angle	rad
λ_{tara}	Vehicle tare	kg	$\dot{\psi}$	Variation rate of yaw angle	$\text{rad} \cdot \text{s}^{-1}$
λ_u	Payload transported by the vehicle	kg	ω'	Angular slip speed when braking per unit length	$\text{rad} \cdot \text{s}^{-1} \cdot \text{m}^{-1}$
μ	Dynamic friction coefficient (or adhesion coefficient)	Ø			

Appendix B

Hertz's formulation is presented next:

$$A = \frac{1}{2}\left(\frac{1}{R_{y_1}} + \frac{1}{R_{y_2}}\right) \tag{A1}$$

$$B = \frac{1}{2}\left(\frac{1}{R_{x1}} + \frac{1}{R_{x2}}\right) \tag{A2}$$

$$R_{y_2} = \frac{r}{cos\gamma_o} \tag{A3}$$

$$A_c = \pi a b \tag{A4}$$

$$a = m_H \left(\frac{3}{2}N\frac{1-v^2}{E}\frac{1}{A+B}\right)^{\frac{1}{3}} \tag{A5}$$

$$b = n_H \left(\frac{3}{2}N\frac{1-v^2}{E}\frac{1}{A+B}\right)^{\frac{1}{3}} \tag{A6}$$

$$\frac{1-v^2}{E} = \frac{1}{2}\left(\frac{1-v_1^2}{E_1} + \frac{1-v_2^2}{E_2}\right) \tag{A7}$$

$$cos\theta = \frac{|B-A|}{A+B} \tag{A8}$$

$$p_{z_o} = \frac{3F_z}{2\pi a b} \tag{A9}$$

$$\delta_o = r_H \left(\left(\frac{3}{2}N\frac{1-v^2}{E}\right)^2 (A+B)\right)^{\frac{1}{3}} \tag{A10}$$

Appendix C

Table A3. Input values common to the three scenarios (920 and 355 mm wheels).

Variable	Value	Variable	Value	Variable	Value
A_f (Ø)	0.400	K (*flange*) (Ø)	1.235–2.747	γ_o (*tread*) (°)	1.432
B_f (s/m)	0.600	k_A (Ø)	1	γ_o (*tread'*) (°)	1.432
e (m)	1.800	k_S (Ø)	0.400	γ_o (*flange*) (°)	51–70
E_1 (Pa)	2.100×10^{11}	R_{x_1} (*tread*) (m)	300×10^{-3}	η (m)	0.007
E_2 (Pa)	2.100×10^{11}	R_{x_1} (*tread'*) (m)	80×10^{-3}	λ_{tara} (kg)	20,000
g (m·s^{-2})	9.810	R_{x_1} (*flange*) (m)	13×10^{-3}	μ (Ø)	0.400
G_1 (Pa)	81.712×10^9	R_{x_2} (*tread*) (m)	5×10^7	μ_o (Ø)	0.550
G_2 (Pa)	81.712×10^9	R_{x_2} (*tread'*) (m)	5×10^7	v_1 (Ø)	0.285
H_{tara} (m)	0.512	R_{x_2} (*flange*) (m)	$(13 \text{ or } 20) \times 10^{-3}$	v_2 (Ø)	0.285
H_{CdG} (m)	1.573	n_{dec} (Ø)	0	ρ (kg·m^{-3})	7850
J (m)	1.668	o (m)	0.075	τ_{lm} (Pa)	3.120×10^8
k(*tread*) (Ø)	0.025	w_w (m)	0.140		
k(*tread'*) (Ø)	0.025	α_{fn} (Ø)	0.750		

Notes: (1) Tread' is the tread of the wheel opposed to the wheel experiencing flange–rail contact. (2) Some values are expressed as ranges since flange–rail contact geometry is a little different at every contact. (3) The 5×10^7 means that the value tends to infinity (∞ is not accepted on EES).

Appendix D

Table A4. Extent of RCF and wear for the two different wheels when flange-rail contact occurs.

Variable	920 mm Wheel	355 mm Wheel
D (m)	0.920	0.355
e (m)	1.800	1.800
λ_{eje} (kg)	18,784	6996
R (m)	265	265
F_{surf} ($\emptyset$)	0.433	0.409
p_{z_o} (Pa)	6.401×10^9	6.584×10^9
$T\gamma$ (N)	468.088	367.887
a (mm)	10.030	6.276
b (mm)	0.636	0.881
A_c (mm^2)	20.031	17.360
$T\gamma/A_c$ (N/mm^2)	23.368	21.192
$W_R, USFD\left(\frac{\mu g}{m \times mm^2}\right)$	55	55
H_{USFD} (μm)	2.295	3.538
F_x (N)	1274	1009
F_y (N)	41,159	34,760
M_z (N $\times$ m)	197.200	55.28
v_x ($\emptyset$)	-3.013×10^{-3}	-2.581×10^{-3}
v_y ($\emptyset$)	-5.760×10^{-3}	-5.760×10^{-3}
$\varphi\left(\frac{rad}{m}\right)$	1.152	-2.986
N (N)	85,465	76,224

Notes: Values for the flange.

References

1. Ministerio de Fomento; Ministère de l'Environnement, de l'Énergie et de la Mer. Servicios de Autopista Ferroviaria (AF) en los Ejes Atlántico y Mediterráneo. Convocatoria de Manifestaciones de Interés. Consulta a los Fabricantes y Diseñadores de Material Móvil. Report. 2018. Available online: https://www.ecologie.gouv.fr/sites/default/files/180410_AMI_Constructeurs_rapport_ES-min.pdf (accessed on 19 June 2024). (In Spanish)
2. Jaro, L.; Folgueira, C.A. Las Autopistas ferroviarias: ¿Una apuesta de futuro en líneas mixtas de alta velocidad? *Rev. Alta Velocidad* **2012**, *2*, 73–96.
3. European Council. Directive 96/53. *Off. J. Eur. Communities* **1996**, *L235*, 59–79.
4. Ministerio de Fomento. Orden FOM/1630/2015, de 14 de julio, por la que se aprueba la "Instrucción ferroviaria de gálibos". *Boletín Estado* **2015**, *185*.
5. Cui, D.; Zhang, W.; Tian, G.; Li, L.; Wen, Z.; Jin, X. Designing the key parameters of EMU bogie to reduce side wear of rail. *Wear* **2016**, *366–367*, 49–59. [CrossRef]
6. Corrêa, P.H.A.; Ramos, P.G.; Fernandes, R.; Kurka, P.R.G.; dos Santos, A.A. Effect of primary suspension and friction wedge maintenance parameters on safety and wear of heavy-haul rail vehicles. *Wear* **2023**, *524–525*, 204748. [CrossRef]
7. Zhai, W.; Jin, X.; Wen, Z.; Zhao, X. Wear Problems of High-Speed Wheel/Rail Systems: Observations, Causes, and Countermeasures in China. *ASME. Appl. Mech. Rev.* **2020**, *72*, 060801. [CrossRef]
8. Wang, H.; Han, J.; Su, M.; Wan, S.; Zhang, Z. The relationship between freight transport and economic development: A case study of China. *Res. Transp. Econ.* **2021**, *85*, 100885. [CrossRef]
9. Seo, J.-W.; Hur, H.-M.; Kwon, S.-J. Effect of Mechanical Properties of Rail and Wheel on Wear and Rolling Contact Fatigue. *Metals* **2022**, *12*, 630. [CrossRef]
10. Sang, H.; Zeng, J.; Qi, Y.; Mu, J.; Gan, F. Study on wheel wear mechanism of high-speed train in accelerating conditions. *Wear* **2023**, *516–517*, 204597. [CrossRef]
11. Soleimani, H.; Moavenian, M. Tribological Aspects of Wheel–Rail Contact: A Review of Wear Mechanisms and Effective Factors on Rolling Contact Fatigue. *Urban Rail Transit* **2017**, *3*, 227–237. [CrossRef]
12. Hewan, G.Y.; Redda, D.T.; Mohammedseid, A. Influence of Axle Load on the Wear of Railway Wheel Material. *Model. Simul. Eng.* **2023**, *2023*, 6730640. [CrossRef]
13. Fissette, P. Railway Vehicle Dynamics. Teaching Content. Catholic University of Louvain, Louvain. 2016. Available online: https://es.scribd.com/document/559372304/RailVehicles (accessed on 19 June 2024).
14. Larrodé, E. *Ferrocarriles y Tracción Eléctrica*, 1st ed.; Editorial Copy Center: Zaragoza, Spain, 2007.
15. Moody, J.C. Critical Speed Analysis of Railcars and Wheelsets on Curved and Straight Track. Bachelor's Thesis, Bates College, Lewison, ME, USA, 2014. Available online: https://core.ac.uk/download/pdf/230689735.pdf (accessed on 19 June 2024).

16. Pellicer, D.S.; Larrodé, E. Analysis of the Rolling Phenomenon of a Reduced-Diameter Railway Wheel for Freight Wagons, as a Function of Operating Factors. Master's Thesis, University of Zaragoza, Zaragoza, Spain, 2021. Available online: https://deposita.unizar.es/record/64448 (accessed on 19 June 2024). (In Spanish)
17. Oldknow, K. Wheel—Rail Interaction Fundamentals. Course Content. 2015. Available online: https://www.coursehero.com/file/185769149/PC-1-3-Wheel-Rail-Interaction-Fundamentals-WRI-2017-20170604pdf/ (accessed on 19 June 2024).
18. Ortega, E. Simulación del Contacto Rueda-Carril con Pro/ENGINEER. Bachelor's Thesis, Universidad Carlos III, Madrid, España, 2012. Available online: https://e-archivo.uc3m.es/entities/publication/1ad42047-7a29-4236-a081-52f4c2ec2646 (accessed on 19 June 2024). (In Spanish)
19. RENFE. Temario Específico para las Pruebas Presenciales de la Especialidad Máquinas-Herramientas. Material de Studio. 2020. Available online: https://www.renfe.com/content/dam/renfe/es/Grupo-Empresa/Talento-y-personas/Empleo/2024/ingenier%C3%ADa-y-mantenimiento/04.%20IYM%20Manual_%20Especialidad_Maquinas_Herramientasv2.pdf (accessed on 19 June 2024).
20. Rovira, A. Modelado del Contacto Rueda-Carril para Aplicaciones de Simulación de Vehículos Ferroviarios y Estimación del Desgaste en el Rango de Baja Frecuencia. Ph.D. Thesis, Polytechnical University of Valencia, Valencia, Spain, 2012. Available online: https://riunet.upv.es/handle/10251/14671 (accessed on 19 June 2024).
21. Sichani, M.S. On Efficient Modelling of Wheel-Rail Contact in Vehicle Dynamics Simulation. Ph.D. Thesis, KTH Institute of Technology, Stockholm, Sweden, 2016. Available online: https://kth.diva-portal.org/smash/record.jsf?dswid=6030 (accessed on 19 June 2024).
22. AENOR. *Aplicaciones Ferroviarias. Ruedas y Carriles*; AENOR: Madrid, Spain, 2011–2021.
23. ADIF. *Calificación, Geometría, Montaje y Diseño de la vía*; ADIF: Madrid, Spain, 1983–2021.
24. ADIF. Declaración sobre la Red. *Annual Report.* 2023. Available online: https://www.adif.es/sobre-adif/conoce-adif/declaracion-sobre-la-red (accessed on 19 June 2024). (In Spanish)
25. Andrews, H.I. *Railway Traction: The Principles of Mechanical and Electrical Railway Traction*, 1st ed.; Elsevier Science: Oxford, UK, 1986.
26. Santamaría, J.; Vadillo, E.G.; Gómez, J. Influence of creep forces on the risk of derailment of railway vehicles. *Veh. Syst. Dyn.* **2009**, *47*, 721–752. [CrossRef]
27. Tipler, P.A.; Mosca, G. *Physics for Scientists and Engineers Volume I*, 6th ed.; Macmillan Education: London, UK, 2014.
28. Greenwood, J.A. Hertz theory and Carlson elliptic integrals. *J. Mech. Phys. Solids* **2018**, *119*, 240–249. [CrossRef]
29. Hertz, H.R. Über die Berührung fester elastischer Körper. *J. Reine Angew. Math.* **1882**, *92*, 156–171. [CrossRef]
30. Polach, O. A Fast Wheel—Rail Forces Calculation Computer Code. *Veh. Syst. Dyn.* **2000**, *33*, 728–739. [CrossRef]
31. Polach, O. Creep forces in simulations of traction vehicles running on adhesion limit. *Wear* **2005**, *258*, 992–1000. [CrossRef]
32. Kalker, J.J. *Rolling Contact Phenomena—Linear Elasticity*; CISM International Centre for Mechanical Sciences; Springer: Vienna, Austria, 2000; Volume 411.
33. Piotrowski, J.; Chollet, H. Wheel—Rail contact models for vehicle system dynamics including multi-point contact. *Veh. Syst. Dyn.* **2005**, *43*, 455–483. [CrossRef]
34. Dirks, B.; Enblom, R.; Ekberg, A.; Berg, M. The development of a crack propagation model for railway wheels and rails. *Fatigue Fract. Eng. Mater. Struct.* **2015**, *18*, 1478–1491. [CrossRef]
35. Alba, M.V. Optimización de la Política de Reperfilado de Ruedas para el Citadis 302, en la explotación de Metro Ligero Oeste. *Rev. Libre Técnica* **2015**, *9*, 29–38.
36. Peng, B.; Iwnicki, S.; Shackleton, P.; Crosbee, D. Comparison of wear models for simulation of railway wheel polygonization. *Wear* **2019**, *436–437*, 203010. [CrossRef]
37. Klein, S.A. Development and integration of an equation-solving program for engineering thermodynamics courses. *Comput. Appl. Eng. Educ.* **1993**, *1*, 265–275. [CrossRef]
38. Vera, C. Proyecto Constructivo de una Línea Ferroviaria de Transporte de Mercancías y su Conexión a la Red Principal. Bachelor's Thesis, University of Seville, Seville, Spain, 2015. Available online: https://idus.us.es/handle/11441/44482 (accessed on 19 June 2024). (In Spanish)
39. Pellicer, D.S.; Larrodé, E. Supplementary Material of "Sensitivity Analysis for Low-Floor Wagons". Mendeley Data, 3rd Version. 2024. Available online: https://data.mendeley.com/datasets/8dfxgyvk99/3 (accessed on 9 July 2024).